

# WhisperNet: A Scalable Solution for Bandwidth-Efficient Collaboration

Gong Chen<sup>1</sup> Chaokun Zhang<sup>2\*</sup> Xinyan Zhao<sup>2</sup>

<sup>1</sup>School of Computer Science and Technology, Tianjin University

<sup>2</sup>School of Cybersecurity, Tianjin University

## Abstract

Collaborative perception is vital for autonomous driving yet remains constrained by tight communication budgets. Earlier work reduced bandwidth by compressing full feature maps with fixed-rate encoders, which adapts poorly to a changing environment, and it further evolved into spatial selection methods that improve efficiency by focusing on salient regions, but this object-centric approach often sacrifices global context, weakening holistic scene understanding. To overcome these limitations, we introduce WhisperNet, a bandwidth-aware framework that proposes a novel, receiver-centric paradigm for global coordination across agents. Senders generate lightweight saliency metadata, while the receiver formulates a global request plan that dynamically budgets feature contributions across agents and features, retrieving only the most informative features. A collaborative feature routing module then aligns related messages before fusion to ensure structural consistency. Extensive experiments show that WhisperNet achieves state-of-the-art performance, improving AP@0.7 on OPV2V by 2.4% with only 0.5% of the communication cost. As a plug-and-play component, it boosts strong baselines with merely 5% of full bandwidth while maintaining robustness under localization noise. These results demonstrate that globally-coordinated allocation across what and where to share is the key to achieving efficient collaborative perception.

## 1. Introduction

Collaborative perception (CP) enhances autonomous driving safety through vehicle-to-everything (V2X) communication [12] to overcome single-agent limitations like occlusions [15, 30]. However, these benefits incur substantial communication overhead, as transmitting raw sensor data or high-dimensional features [4] in real-time consumes a vast amount of bandwidth. This bandwidth constraint has become a critical bottleneck, hindering the large-scale deployment of CP [7, 19]. Therefore, designing communication-

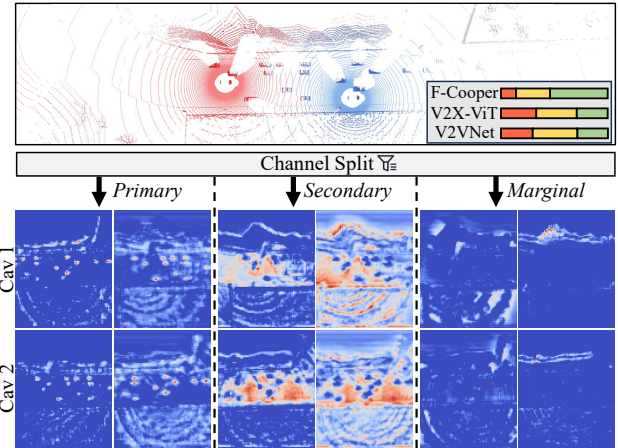


Figure 1. Visualization of different channel groups. The proportional table in the figure represents the model’s primary (Orange), secondary (Yellow), and marginal (Green) channels.

efficient methods that maintain high perception accuracy under strict bandwidth budgets remains a challenge.

To mitigate bandwidth, prior work mainly follows two strategies. First, **feature compression & reconstruction methods** [11, 23] encode the full feature map into a compact latent and decode it at the receiver; however, fixed-rate encoders or static codebooks are inflexible, failing to adapt to dynamic bandwidth and varying scene complexity [34], thus enforcing a fidelity-bandwidth compromise. To gain more flexibility, **spatial selection methods** [10, 33] are proposed to reduce bandwidth by transmitting only salient spatial features. For instance, methods like Where2comm [10] and CoRA [2] prioritize foreground objects.

However, while spatial-only methods optimize where to communicate, they still transmit full, redundant channels. Even recent filtering methods [31] may not fully exploit this redundancy on a global, system-wide scale. This reveals a critical gap: existing methods have overlooked the significant redundancy present in the channel dimension. This gap motivates our investigation into the channel properties. As shown in Fig. 1, channels can be qualitatively grouped into three categories: primary channels, which are

\*Corresponding author.

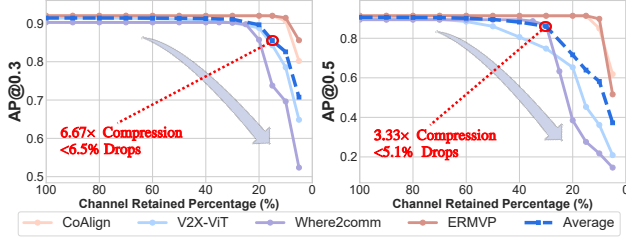


Figure 2. Impact of Channel Pruning on Performance.

crucial for defining objects; secondary channels, which provide complementary contextual details; marginal channels, which are largely redundant. Transmitting these marginal channels not only wastes valuable bandwidth but can also introduce noise that degrades perception accuracy. We validate this hypothesis with a preliminary experiment. By ranking channels based on their post-fusion  $L1$ -norm [26] and pruning the unimportant ones, we observe a striking result (Fig. 2): Removing nearly half of the channels does not harm performance. This finding confirms the unexploited potential of channel redundancy and underscores the need for a more principled, content-aware allocation strategy.

While prior methods have mainly focused on selecting spatial regions, our findings on channel redundancy reveal that this addresses only half of the problem. This leads to our core insight: an effective communication strategy must jointly optimize *where* to communicate and *what* to transmit. To this end, we present WhisperNet, a novel framework that actualizes this optimization via a globally-coordinated allocation scheme. This scheme formulates a holistic plan for feature exchange based on system-wide metadata, ensuring a complementary fusion. WhisperNet comprises three key modules. 1) Sender-side Importance Estimation Module, which employs a lightweight attention mechanism to jointly estimate spatial and channel importance maps for transmission; 2) Receiver-side Confidence-Aware Module, which acts as the global coordinator, gathering all metadata to formulate a global request plan that dynamically budgets feature contributions across agents and features; 3) Collaborative Feature Routing Module, which aligns the received messages by directing related subsets to specialized sub-networks, enabling context-aware integration. Experiments demonstrate WhisperNet’s superiority. When limited to only 1% bandwidth, it surpasses the second-best method’s accuracy by 10.6%/11.7% on OPV2V/DAIR-V2X. Moreover, its plug-and-play design enables seamless integration into existing models, reducing their communication cost by 95% on average with negligible accuracy loss.

Our contributions are summarized as follows: (1) We tackle the critical problem of redundancy in CP by proposing a novel paradigm that shifts from sender-side filtering to receiver-centric global coordination; (2) We design Whis-

perNet, a lightweight module that can integrate with existing methods to achieve significant communication reduction at a negligible performance cost. (3) Extensive experiments verify our state-of-the-art approach for performance-bandwidth trade-off under strict constraints.

## 2. Related Work

**Collaborative Perception.** CP enables agents to achieve perceptual capabilities beyond those of a single vehicle by sharing messages. Mainstream approaches fall into three categories: Early fusion [4, 21] directly transmits raw perception data, offering high accuracy but incurring immense bandwidth overhead. Methods like Cooper [4], which performs 3D object detection by aggregating multi-vehicle point clouds. Late fusion [1, 5] minimizes the communication burden by only exchanging detection results, but its robustness is limited under occlusion and in blind spots. For instance, Coop3D [1] implements vehicle-infrastructure collaborative detection via a result-level sharing method. Positioned between these two, intermediate fusion [22, 28, 31] strikes a balance between accuracy and bandwidth by sharing intermediate features. Among these methods, V2X-ViT [28] utilizes heterogeneous multi-agent attention and multi-scale window attention to model cross-agent interaction and spatio-temporal alignment, while V2VNet [25] implements feature-level fusion with a graph attention and message-passing mechanism. Nevertheless, the bandwidth required by intermediate fusion schemes remains a key bottleneck, which constrains their large-scale deployment.

**Multi-agent Communication.** Earlier approaches reduce bandwidth by holistically compressing intermediate features on the sender and reconstructing them on the receiver. Typical designs include cooperative reconstruction with a compressor-decoder like AttFuse [29] and CORE [23]. While effective at lowering volume, these schemes rely on static encoders or codebooks [6, 11], limiting adaptability to dynamic bandwidth and scene complexity. Who2com [17] and When2com [16] learn which partners to talk to and when to form groups, typically sending full features once selected. This reduces traffic via selective partner/time scheduling but struggles to scale as the number of agents grows. Recent methods improve the bandwidth-accuracy trade-off via two primary strategies: one-stage [31, 33] or two-stage [2, 10, 27] protocols. One-stage spatial methods directly send salient tiles. For example, How2comm [31] combines feature filtering and pragmatic fusion for direct transmission. Two-stage protocols first exchange needs, then transmit features accordingly. For example, Where2comm [10] introduced spatial confidence maps to send only salient regions; subsequent CoSDH [27] models supply-demand hybridization. However, these methods remain largely ego-centric or pairwise in their decision-making. For instance, CoSDH’s pairwise allocation can still

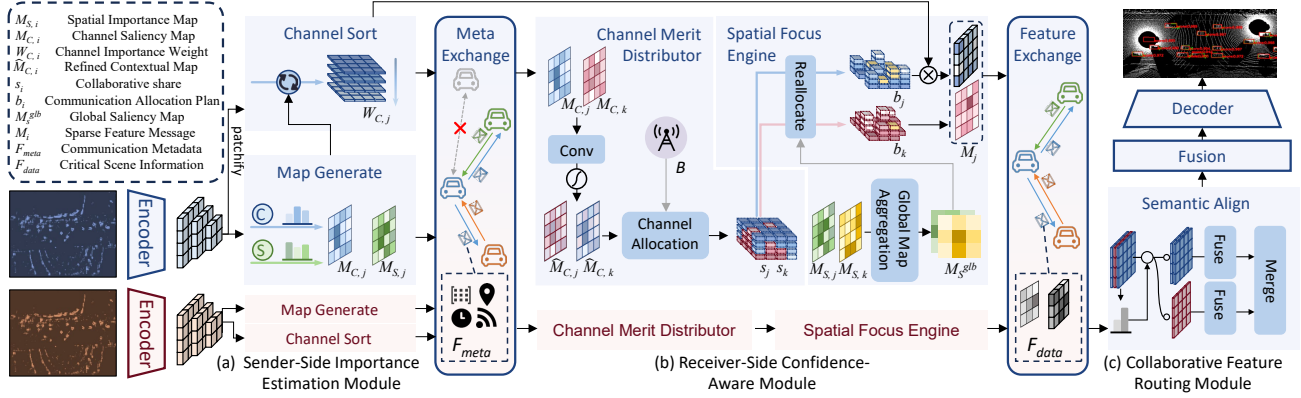


Figure 3. The architecture of WhisperNet. Each sender agent first extracts features from its raw sensor data and generates compact importance maps that summarize both spatial and channel-wise saliency. These maps are then exchanged with a receiver agent, which dynamically requests only the most critical feature subsets. Finally, the requested features are fused by a collaborative routing module.

miss the global optimum, leading to duplicated uploads for the same region or, conversely, gaps where no one uploads. This motivates a globally coordinated scheme that jointly decides, for every region, who should transmit and how to avoid redundancy while preserving scene completeness.

### 3. Methods

#### 3.1. Methodology Overview

**Problem Formulation.** We consider a system of  $N$  agents,  $\mathcal{V} = \{1, \dots, N\}$ , including the ego agent  $i$ , operating over  $K$  communication rounds. In each round  $k \in \{1, \dots, K\}$ , each agent  $j \in \mathcal{V}$  extracts a local feature map  $X_j$  from its sensors. The agent then utilizes its communication module  $\mathcal{C}$  to generate and exchange a set of messages, denoted as  $\mathbb{M}_j^{(k)}$  with other agents. The total communication process is constrained by a bandwidth budget  $B_j$  for each agent. The goal is to design an optimal communication module  $\mathcal{C}$  that maximizes the perception performance  $\mathcal{P}$  for any agent  $j$  with fusion module  $\mathcal{F}$  under the given bandwidth constraints. This optimization problem is expressed as:

$$\begin{aligned} & \underset{\mathcal{C}}{\text{maximize}} \quad \mathcal{P}\left(\mathcal{F}\left(X_i, \{\mathbb{M}_j^{(k)}\}_{j \neq i, \forall k}\right)\right) \\ & \text{s.t.} \quad \sum_{k=1}^K \text{Size}(\mathbb{M}_j^{(k)}) \leq B_j, \forall j \in \mathcal{V} \end{aligned} \quad (1)$$

**Framework Overview.** As shown in Fig. 3, WhisperNet implements the communication module  $\mathcal{C}$  through three modules. 1) Sender-Side Importance Estimation Module: This module analyzes the local feature map to generate a spatial-channel importance map that summarizes the agent’s information. 2) Receiver-Side Confidence-Aware Module: It gathers importance maps from other agents, creating a dynamic communication plan and requesting the most critical data across all agents. 3) Collaborative Feature Routing Module: This module performs channel-wise

alignment of the sparse features from all agents, serving as a preparation step for downstream fusion.

#### 3.2. Sender-Side Importance Estimation Module

The role of the Sender-Side Importance Estimation module is to analyze the local feature  $X_j \in \mathbb{R}^{H \times W \times C}$  and generate a joint importance map for transmission that guides the coordination by highlighting the spatial and channel-wise locations of the most salient features. The module’s operation is divided into two primary functions: Map Generation to produce importance maps for transmission and Channel Sort to prepare local channel weights for selection.

**Map Generation.** This function generates two distinct importance maps for transmitting: a spatial importance map  $M_{S,j}$  and a channel saliency map  $M_{C,j}$ . As shown in Fig. 4, the Spatial Importance Predictor identifies critical regions within the feature. It takes the entire feature  $X_j$  as input and outputs a spatial importance  $M_{S,j} \in [0, 1]^{H \times W}$ , where each value indicates the significance of a spatial location. This is achieved using a mapping function  $\mathcal{G}_S$ .

$$M_{S,j} = \mathcal{G}_S(X_j) \quad (2)$$

where  $\mathcal{G}_S$  is implemented as a two-layer convolutional head.

Channel Importance Estimation determines what content is most informative. Motivated by prior work [20, 24], which indicates high-frequency details are more valuable than low-frequency features, our method determines this by scoring the information density of each feature channel.

We first score channels by patch-wise information density. For the  $c$ -th channel  $X_{j,c} \in \mathbb{R}^{H \times W}$ , we divide it into patches  $\{p_{j,c}^k\}_{k=1}^Q$  with  $Q = \frac{H}{P} \cdot \frac{W}{P}$  to preserve feature coherency. We then compute a Laplacian magnitude score for each patch to derive its informativeness:

$$S(p_{j,c}^k) = \|\nabla^2 p_{j,c}^k\|_1 = \sum_{(u,v) \in \mathcal{P}_k} |(\mathcal{L} * X_{j,c})_{u,v}| \quad (3)$$

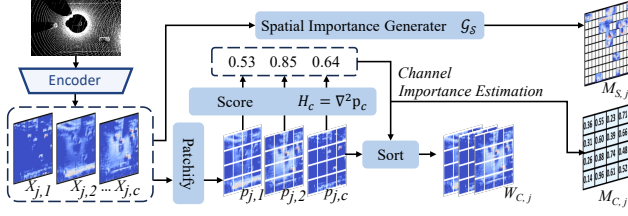


Figure 4. Sender-Side Importance Estimation module. It evaluates feature from both spatial and channel perspectives to generate importance maps that guides communication coordination.

where  $\mathcal{L}$  is a  $3 \times 3$  Laplacian kernel and  $\mathcal{P}_k$  denotes the pixel index set of the  $k$ -th patch. From these patch scores, we then generate a 2D channel saliency map  $M_{C,j}$ .

For each patch location  $k$ , we classify channels into three groups primary, secondary, and marginal using a lightweight  $1 \times 1$  conv head to generate three classification scores for each channel, followed by a softmax over the three groups, yielding the resulting group probabilities  $\pi_{j,k,c} = [\pi_{j,k,c}^{\text{pri}}, \pi_{j,k,c}^{\text{sec}}, \pi_{j,k,c}^{\text{mar}}]^\top$  for channel  $c$ . We further let  $\omega = [\omega_{\text{pri}}, \omega_{\text{sec}}, \omega_{\text{mar}}]^\top$  be learnable group weights. We compute the group-weighted channel saliency map  $M_{C,j}$  for transmission by taking the normalized maximum score at each patch  $k$ :

$$M_{C,j}(k) = \max_c [(\omega^\top \pi_{j,k,c}) S(p_{j,c}^k)]. \quad (4)$$

**Channel Sort.** In parallel, we form a channel weights for local use. For patch  $k$ , we collect channel scores into a vector  $\mathbf{s}_{j,k} = [S(p_{j,1}^k), \dots, S(p_{j,c}^k)]^\top$  and compute weights.

$$\mathbf{w}_{j,k} = \text{Softmax}(\mathbf{s}_{j,k}) \quad (5)$$

The collection of these weights  $W_{C,j} = \{\mathbf{w}_{j,k}\}_{k=1}^Q$  is retained by the sender and not transmitted. These weights will be used later by the coordinator to select the most salient channels. Finally, the importance maps  $M_{S,j}$  and  $M_{C,j}$  are transmitted to the receivers for further processing.

### 3.3. Receiver-Side Confidence-Aware Module

As depicted in the middle of the Fig. 3, the Receiver-Side Confidence-Aware Module works as the ego-centric coordinator and is responsible for intelligently distributing the communication budget  $B$  in each cycle. It adopts a global request-response protocol. The process begins when the ego receives the spatial maps  $\{M_{S,j}\}_{j \neq i}$  and channel maps  $\{M_{C,j}\}_{j \neq i}$  from all collaborators.

To assess the relative importance of each collaborator's information at different locations, the coordinator employs a Channel Merit Distributor. The distributor refines the raw channel saliency maps using a function  $\mathcal{H}$ :

$$\hat{M}_{C,j} = \mathcal{H}(\{M_{C,l}\}_{l \neq i}) \quad (6)$$

Here,  $\mathcal{H}$  consists of a convolutional layer followed by a Gaussian filter, enabling inter-agent interaction and smoothing. The refined map  $\hat{M}_{C,j}$  represents the contextual importance of agent  $j$ . Based on this, the collaborative share  $s_{j,k}$  for vehicle  $j$  at patch  $k$  is defined as:

$$s_{j,k} = \frac{\hat{M}_{C,j}(k)}{\sum_{l \neq i} \hat{M}_{C,l}(k) + \epsilon} \quad (7)$$

However, allocating the budget uniformly across all patches and then distributing it by shares  $s_{j,k}$  is suboptimal, as background regions require fewer resources than critical areas. To address this, we introduce a Spatial Focus Engine, which redistributes the budget according to spatial importance maps  $\{M_{S,j}\}_{j \neq i}$ . We first generate a unified global saliency map  $M_S^{\text{global}}$  by taking the element-wise maximum of all individual spatial maps. This global map is then transformed into a spatial budget distribution  $P_S$ :

$$P_S(k) = \frac{\exp(M_S^{\text{global}}(k)/\tau_s)}{\sum_{k'=1}^Q \exp(M_S^{\text{global}}(k')/\tau_s)} \quad (8)$$

With  $P_S(k)$ , the budget for each patch  $k$  is computed as:

$$\hat{B}_{\text{patch}}(k) = B \cdot P_S(k) \quad (9)$$

For each patch  $k$ , the coordinator first allocates the patch budget  $\hat{B}_{\text{patch}}(k)$  to all agents in proportion to their collaborative shares  $s_{j,k}$ :

$$b_{j,k} = \left[ \hat{B}_{\text{patch}}(k) \cdot s_{j,k} \right]. \quad (10)$$

The resulting allocation matrix  $\{b_{j,k}\}$  is then broadcast to all collaborators. Upon receiving the allocation plan, each agent  $j$  locally prioritizes its transmission according to the channel groups and  $W_{C,j}$ : primary channels are sent first, followed by secondary, while marginal channels are only transmitted when remaining bandwidth allows.

### 3.4. Collaborative Feature Routing Module

This module serves as a channel alignment and organization layer that harmonizes the sparse features received from all agents before the subsequent fusion stage. Instead of directly performing feature fusion, the module focuses on routing semantically correlated channels into coherent groups, ensuring that information distributed across different agents is well-aligned for downstream integration.

As shown in Fig. 5, the sparse feature messages  $\{M_j\}_{j \in \mathcal{N}}$  are first combined into a unified tensor  $X_{\text{in}} \in \mathbb{R}^{N \times C \times H \times W}$  by zero-padding the unselected channels. For each channel  $c$ , a routing network generates a soft assignment vector  $\mathbf{g}_c \in \mathbb{R}^m$ , indicating its affinity to  $m$  specialized experts.

$$\mathbf{g}_c = \text{Softmax}(\text{MLP}(\text{GlobalAvgPool}(X_{\text{in}}^c))). \quad (11)$$

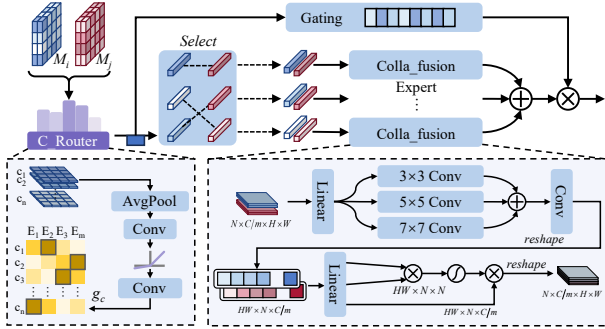


Figure 5. Collaborative Feature Routing module. It enables cross-vehicle feature exchange by grouping and processing semantically similar channels.

Each input channel is assigned to the expert with the highest affinity, which enables semantic grouping, avoiding indiscriminate direct fusion.

Within each expert, a lightweight multi-scale convolutional block with parallel  $3 \times 3$ ,  $5 \times 5$ , and  $7 \times 7$  kernels refines local structures to normalize and align intra-agent representations, preparing them for consistent downstream processing. An attention-based inter-agent recalibration step is then applied along the agent dimension, adapting per-channel alignment to reduce cross-agent inconsistency. Finally, the outputs of all  $m$  experts are recombined through element-wise summation to restore the aligned feature tensor. This pathway operates in parallel with a residual Squeeze-and-Excitation [9] branch applied to  $X_{in}$  for global channel recalibration. The output provides a channel-harmonized representation that facilitates stable and efficient fusion in the following Fusion module.

## 4. Experiments

### 4.1. Experimental Settings

**Datasets.** We evaluate our method on two large-scale datasets: OPV2V [29] and DAIR-V2X [32]. OPV2V is the first large-scale open dataset for vehicle-to-vehicle perception. The dataset encompasses 73 diverse scenarios across urban and highway environments that simulate realistic traffic and occlusion conditions. DAIR-V2X is a pioneering large-scale dataset for vehicle-to-infrastructure perception. DAIR-V2X provides synchronized data from both vehicle and infrastructure sensors in real-world traffic scenarios.

**Implementation details.** We follow the standard settings from the OpenCOOD benchmark [29] for both datasets, with a communication range of 70 meters for all agents. For the 3D object detection task, we restrict the point cloud range to  $[-140.8, 140.8] \times [-40, 40] \times [-3, 1]$  meters. We evaluate performance using Average Precision (AP) at Intersection over Union (IoU) thresholds of 0.5 and 0.7 (AP@0.5/AP@0.7). For the semantic segmentation

Table 1. Performance comparison of mainstream methods.

Methods	Params	OPV2V		DAIR-V2X	
		AP@0.5	AP@0.7	AP@0.5	AP@0.7
Single	6.28 M	0.8078	0.6853	0.6250	0.4457
Late	6.28 M	0.8670	0.8025	0.6971	0.5107
Inter.	6.28 M	0.8403	0.6774	0.6506	0.5538
V2VNet [25]	16.08 M	0.9175	0.8221	0.6644	0.4037
V2X-ViT [28]	14.50 M	0.9035	0.8119	0.7046	0.5240
Where2comm [10]	10.43 M	0.8937	0.7889	0.6735	0.5317
CoAlign [18]	11.42 M	0.9132	0.8381	0.7772	0.6284
How2Comm [31]	35.79 M	0.8589	0.7147	0.6236	0.4718
MRCNet [8]	18.79 M	0.8529	0.7698	0.6647	0.5385
DSRC [34]	10.14 M	0.9183	0.8526	0.7852	0.6360
CoSDH [27]	8.52 M	0.8952	0.8373	0.7042	0.5766
ERMVP [33]	11.87 M	0.9139	0.8404	0.7675	0.6350
MDD [13]	8.09 M	0.8007	0.6817	0.7495	0.5817
WhisperNet	7.28 M	0.9334	0.8764	0.7915	0.6480

task, the perception range is  $[-51.2, 51.2] \times [-51.2, 51.2] \times [-3, 1]$  meters. We report the mean Intersection over Union (mIoU) across the Road, Lane, and Vehicle classes. Across all experiments, we use PointPillars [14] as the backbone for feature extraction from point clouds, with a voxel size of 0.4 meters. We adopt the default value of 1 from the softmax function for  $\tau_s$ . The number of experts is set to 4.

Following the OPV2V benchmark, we take the standard intermediate-fusion with  $16 \times$  compression as the reference, and define it as the communication rate of 1.0. All reported rates are measured relative to this baseline.

**Baselines.** We adopt the collaboration model in OPV2V [29] as the baseline for WhisperNet. In our experiments, WhisperNet is extensively compared with a wide range of state-of-the-art communication-efficient methods, such as Where2comm [10], ERMVP [33], and CoSDH [27]. To further assess its plug-and-play capability, WhisperNet is integrated into several representative frameworks: F-Cooper [3], V2VNet [25], and V2X-ViT [28]. We evaluate both the communication efficiency and perception performance under varying bandwidth budgets.

### 4.2. Quantitative Evaluation

**Benchmark Comparison.** Tab. 1 presents the 3D object detection results on the OPV2V and DAIR-V2X benchmarks. Our proposed WhisperNet consistently achieves competitive or even state-of-the-art performance with a substantially smaller model size. Notably, on OPV2V, WhisperNet attains an AP@0.7 of 87.64% while using only 7.28M parameters, which is significantly more compact than previous leading methods such as DSRC (10.02M). A similar trend is observed on DAIR-V2X, where WhisperNet outperforms the runner-up by 1.2% AP@0.7 with fewer parameters. These results indicate that, despite being lightweight and designed to reduce redundant information exchange, WhisperNet can still effectively prioritize the most salient features by jointly modeling spatial and channel importance via its ego-centric coordination scheme.

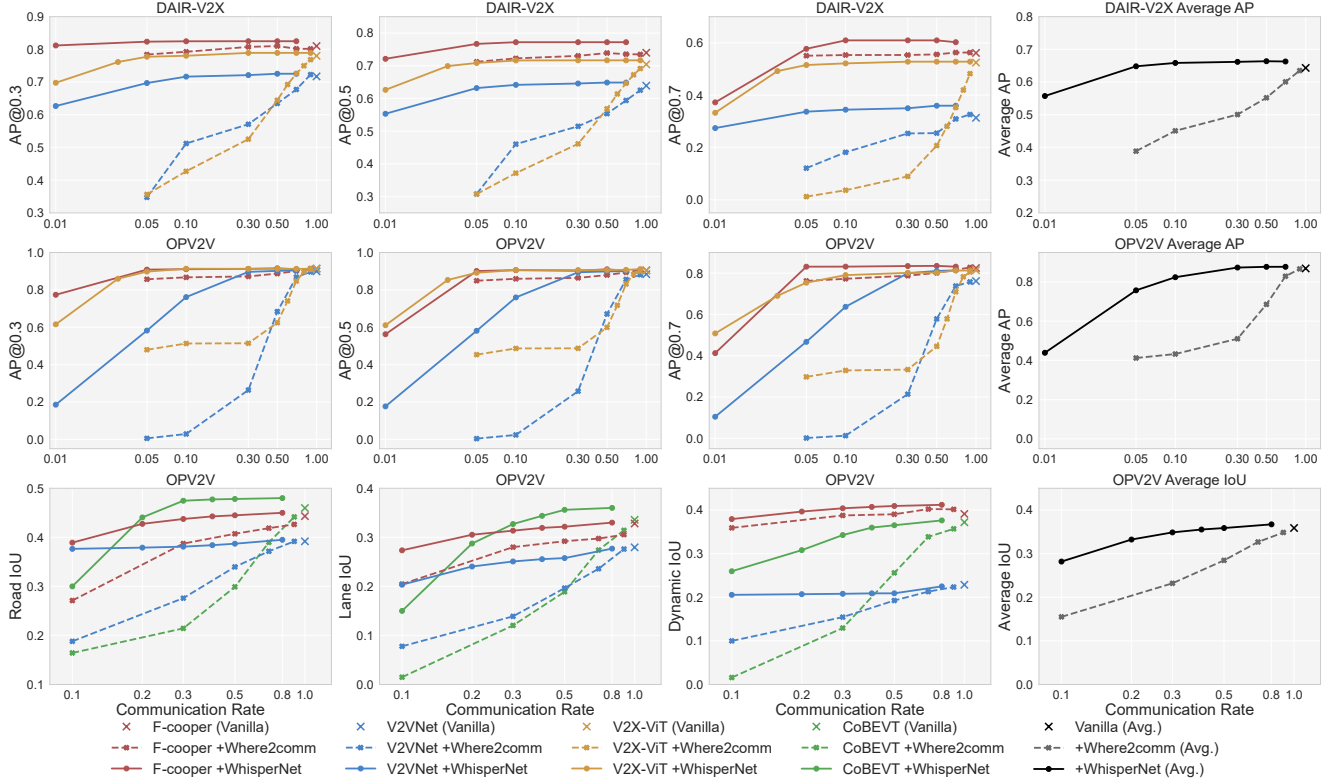


Figure 6. Plug-and-play performance validation. The figure compares the 3D object detection and BEV semantic segmentation performance when using our method (WhisperNet) and Where2comm as communication plug-ins under varying communication rates.

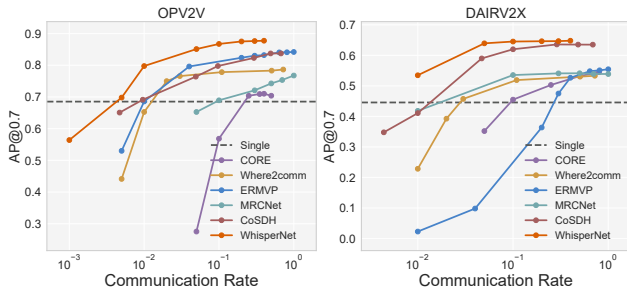


Figure 7. Comparison of performance and bandwidth.

**Performance-Bandwidth Trade-off.** Fig. 7 shows that WhisperNet consistently achieves a leading trade-off between perception accuracy and communication cost. On OPV2V, WhisperNet outperforms the second-best competitor by 4.0% at a 40% communication rate. When the bandwidth is further reduced to only 1%, this advantage becomes more pronounced, with performance gains of 10.6% and 11.7% on OPV2V and DAIR-V2X, respectively. The bandwidth reduction capability of WhisperNet is further demonstrated by its ability to maintain baselines even when operating at only 0.5% of the original bandwidth. In contrast, methods such as CORE, which rely on static feature com-

pression, fail to adapt to extremely limited budgets. This advantage arises from WhisperNet’s cooperative coordination mechanism, which enables all agents to determine what and where to transmit for optimal bandwidth utilization.

**Plug-and-Play Evaluation.** Fig. 6 validates WhisperNet’s plug-and-play capability. When integrated into existing methods, it still offers a superior trade-off between accuracy and communication. For 3D object detection, integrating WhisperNet allows these methods to maintain their full-bandwidth performance while using a fraction of the data. For instance, on OPV2V, V2X-ViT surpasses its baseline with only 10% of the communication volume, while on DAIR-V2X, F-Cooper boosts its average AP from 0.704 to 0.723 with just 5% of the original bandwidth. The advantage is particularly pronounced for dense prediction tasks like BEV semantic segmentation. At a 50% communication rate, WhisperNet’s average IoU is over 50% higher than that of the purely spatial method Where2comm. This result highlights how our joint spatial-channel selection preserves the vital features that spatial methods discard, enabling superior performance at a minimal communication cost.

**Robustness to Noise.** Fig. 8 evaluates methods’ robustness to localization errors. We inject Gaussian noise into collaborator poses, including positional noise and heading noise,

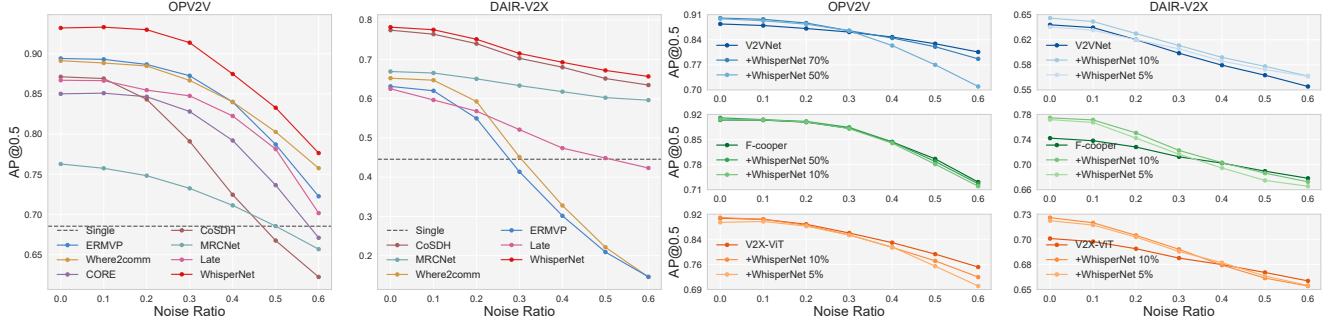


Figure 8. Comparison of model robustness to mixed noise. WhisperNet shows strong resilience compared to baselines, maintaining accuracy under high pose and heading perturbations

both sampled from  $\mathcal{N}(0, \sigma^2)$ . As shown in the first two subfigures of Fig. 8, WhisperNet demonstrates exceptional resilience compared to baselines. For instance, under a high noise level of  $\sigma = 0.6$  on DAIR-V2X, its performance degrades by only 16.0%, in stark contrast to the over 75% drop of methods like ERMVP. The remaining subfigures in Fig. 8 further show that this robustness can be transferred to other existing frameworks through WhisperNet’s plug-and-play capability. The integrated models perform well under moderate noise and maintain respectable performance even under heavy noise. For instance, when integrated into V2X-ViT with just 5% bandwidth, the enhanced model suffers a performance drop of less than 1% under extreme noise, nearly matching the full-bandwidth baseline. These results confirm WhisperNet is both robust and capable of transferring this resilience to other frameworks while cutting bandwidth.

### 4.3. Ablation Studies

**Impact of Core Components.** Taking a transmission limit of under 50% as an example, Tab. 2 analyzes the contribution of major components in WhisperNet. The Channel Merit Distributor (CMD) serves as the core mechanism for communication efficiency. It reduces bandwidth by half while maintaining 0.8532 in AP@0.7 on OPV2V. Further integrating the Spatial Focus Engine (SFE) enhances scene-level coordination, leading to consistent improvements across both datasets. Building upon this, the Collaborative Feature Routing (CFR) module performs channel-wise routing and matching. Finally, the full WhisperNet, which surpasses the baseline over 4.31%/5.73% on OPV2V/DAIR-V2X while cutting bandwidth by more than 50%, demonstrates the synergy between our channel-spatial selection and collaborative routing design.

**Impact of Patch Selection** Tab. 3 analyzes the impact of patch size on the accuracy-speed trade-off. At high bandwidth, a larger 4x4 patch offers a more efficient configuration, providing a 10% FPS increase on OPV2V with only a negligible performance drop. However, this trend re-

Table 2. Ablation on the contribution of core modules.

Configuration			OPV2V		DAIR-V2X	
CMD	SFE	CFR	Comm.	AP@0.5/0.7	Comm.	AP@0.5/0.7
			32.81	0.8926/0.8333	24.00	0.7532/0.5907
		✓	32.81	0.9284/0.8672	24.00	0.7769/0.6315
✓			16.40	0.9206/0.8532	12.00	0.7627/0.6036
✓	✓		15.62	0.9310/0.8683	11.27	0.7741/0.6271
✓	✓	✓	15.62	0.9334/0.8764	11.27	0.7915/0.6480

Table 3. Ablation on the size of the feature block.

AP@0.7 (OPV2V / DAIR-V2X)			
Patch Size	5%	50%	FPS
4	0.7732 / 0.5734	0.8752 / 0.6370	8.89 / 10.94
2	0.8329 / 0.6305	0.8773 / 0.6415	8.19 / 10.14
1	0.8511 / 0.6394	0.8764 / 0.6480	8.04 / 10.02

Table 4. Ablation on the number of experts in our Collaborative Feature Routing module on OPV2V.

Experts	AP@0.5/0.7	Params. (M)	GFLOPs
1	0.9158 / 0.8512	13.13	176.25
2	0.9275 / 0.8681	9.43	140.54
4	0.9334 / 0.8764	7.28	122.68
8	0.9121 / 0.8435	6.66	113.76

verses under stringent communication constraints. At just a 5% communication rate, the fine-grained 1x1 patch outperforms the 4x4 patch, boosting the AP@0.7 by over 7.8%. This result demonstrates that a smaller patch size is critical for achieving fine-grained feature selection and preserving accuracy in low-bandwidth scenarios.

**Analysis on the Number of Experts.** Tab. 4 reveals a clear trade-off in the number of experts used. Performance peaks at four experts, improving upon the single-expert by allowing feature channels to be partitioned for more specialized fusion. However, this trend reverses with eight experts, where performance collapses to 84.35% due to overspecialization, which fragments information and hinders

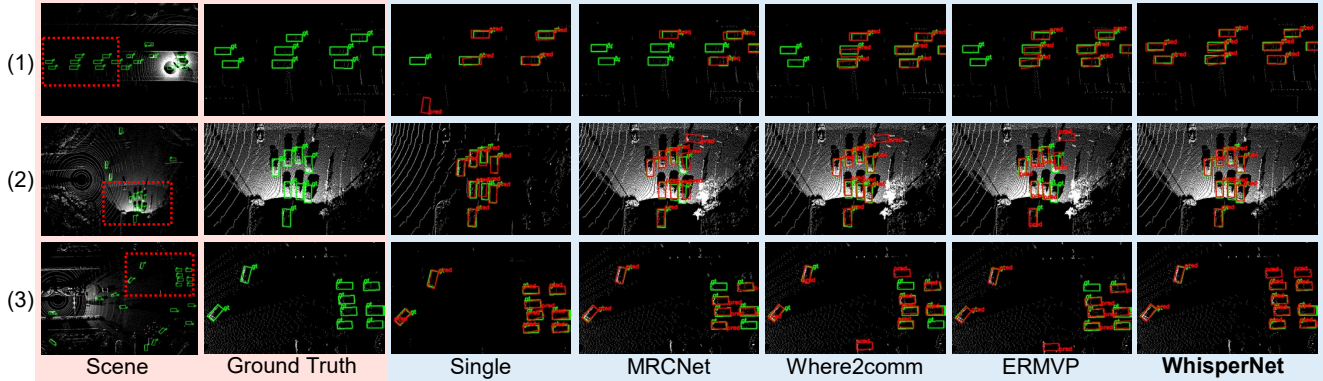


Figure 9. Visualization of mainstream methods in challenging driving scenarios.

Table 5. Ablation on channel importance metrics and patch score aggregation methods on OPV2V.

Type	Multi-Scale			Single-Scale		
	Weighted	Max	Mean	Weighted	Max	Mean
Laplacian	0.8729	0.8709	0.8723	0.8402	0.8388	0.8401
Jacobian	0.8481	0.8467	0.8365	0.8345	0.8327	0.8337
Abs	0.8476	0.8454	0.8394	0.8317	0.8334	0.8317
Max	0.8705	0.8674	0.8669	0.8402	0.8317	0.8301
LSD	0.8533	0.8540	0.8481	0.8392	0.8316	0.8395
Mean	0.8474	0.8629	0.8623	0.8302	0.8017	0.8301

holistic context. We thus adopt four experts as the optimal configuration, as it strikes the best balance between performance, parameter count, and computational cost.

**Analysis of Channel Importance Metric.** Tab. 5 ablates several channel scoring metrics to validate our use of the Laplacian magnitude. We find that metrics capturing high-frequency details through Laplacian responses consistently outperform those based on Jacobian or raw feature statistics (Max/Mean). For aggregation across channels, we evaluate different strategies and adopt a group-weighted formulation, where each channel is weighted by its semantic group importance before taking the maximum. This design achieves the highest 0.8729 AP@0.7, confirming that emphasizing high-frequency and high-confidence channels provides a more reliable indicator of perceptual importance for communication selection.

**Single vs. Multi-Scale Communication.** Fig. 10 further ablates two feature transmission strategies within our framework: Single-Scale, which transmits a single fused intermediate feature, and Multi-Scale, which transmits a richer set of multi-scale features. Multi-Scale strategy is more robust, while the Single-Scale approach is more efficient. The robustness advantage is most pronounced at a 1%, where the Multi-Scale’s AP@0.7 is over 31% higher. Conversely, the Single-Scale approach reduces the data payload by 24% and improves FPS by up to 21%. Given the substantial robustness gains, we adopt the Multi-Scale strat-

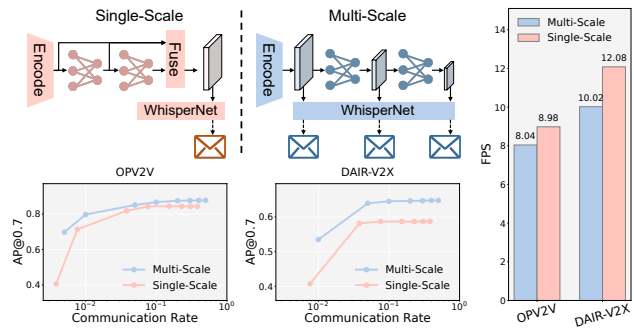


Figure 10. Ablation on single-scale and multi-scale feature transmission strategies.

egy as WhisperNet’s default configuration.

#### 4.4. Qualitative Visualization

Fig. 9 compares our method with baselines in three challenging scenarios featuring occlusion and long-range targets. The single-agent baseline predictably fails to perceive occluded objects. Other collaborative methods improve upon this but still exhibit frequent localization errors and missed detections. In all scenarios, WhisperNet generates significantly cleaner and more accurate results.

#### 5. Conclusion

We presented WhisperNet, a bandwidth-aware collaborative perception framework that jointly optimizes spatial and channel dimensions through a two-sided communication strategy. Experiments show it achieves state-of-the-art performance on major benchmarks while preserving robustness to localization noise and maintaining high efficiency under severe bandwidth constraints. Its effectiveness arises from the coordinated design of sender-side importance estimation, receiver-side adaptive allocation, and collaborative feature alignment, offering a practical solution for scalable and communication-efficient multi-agent perception.

**Acknowledgement.** The work is supported in part by the S&T Program of Hebei Province (Beijing-Tianjin-Hebei Collaborative Innovation Special Program) under Grant 25240701D.

## References

- [1] Eduardo Arnold, Mehrdad Dianati, Robert De Temple, and Saber Fallah. Cooperative perception for 3d object detection in driving scenarios using infrastructure sensors. *IEEE Transactions on Intelligent Transportation Systems*, 23(3): 1852–1864, 2020. 2
- [2] Gong Chen, Chaokun Zhang, Pengcheng Lv, and Xiaohui Xie. Cora: A collaborative robust architecture with hybrid fusion for efficient perception. *arXiv preprint arXiv:2512.13191*, 2025. 1, 2
- [3] Qi Chen, Xu Ma, Sihai Tang, Jingda Guo, Qing Yang, and Song Fu. F-cooper: Feature based cooperative perception for autonomous vehicle edge computing system using 3d point clouds. In *Proceedings of the 4th ACM/IEEE Symposium on Edge Computing*, pages 88–100, 2019. 5
- [4] Qi Chen, Sihai Tang, Qing Yang, and Song Fu. Cooper: Cooperative perception for connected autonomous vehicles based on 3d point clouds. In *2019 IEEE 39th International Conference on Distributed Computing Systems (ICDCS)*, pages 514–524. IEEE, 2019. 1, 2
- [5] Siqi Fan, Haibao Yu, Wenxian Yang, Jirui Yuan, and Zaiqing Nie. Quest: Query stream for practical cooperative perception. In *2024 IEEE International Conference on Robotics and Automation (ICRA)*, pages 18436–18442. IEEE, 2024. 2
- [6] Jiahui Fu, Yue Gong, Luting Wang, Shifeng Zhang, Xu Zhou, and Si Liu. Generative map priors for collaborative bev semantic segmentation. In *Proceedings of the Computer Vision and Pattern Recognition Conference*, pages 11919–11928, 2025. 2
- [7] Yushan Han, Hui Zhang, Huifang Li, Yi Jin, Congyan Lang, and Yidong Li. Collaborative perception in autonomous driving: Methods, datasets, and challenges. *IEEE Intelligent Transportation Systems Magazine*, 15(6):131–151, 2023. 1
- [8] Shixin Hong, Yu Liu, Zhi Li, Shaohui Li, and You He. Multi-agent collaborative perception via motion-aware robust communication network. In *Proceedings of the IEEE/CVF Conference on Computer Vision and Pattern Recognition*, pages 15301–15310, 2024. 5
- [9] Jie Hu, Li Shen, and Gang Sun. Squeeze-and-excitation networks. In *Proceedings of the IEEE conference on computer vision and pattern recognition*, pages 7132–7141, 2018. 5
- [10] Yue Hu, Shaoheng Fang, Zixing Lei, Yiqi Zhong, and Siheng Chen. Where2comm: Communication-efficient collaborative perception via spatial confidence maps. *Advances in neural information processing systems*, 35:4874–4886, 2022. 1, 2, 5
- [11] Yue Hu, Juntong Peng, Sifei Liu, Junhao Ge, Si Liu, and Siheng Chen. Communication-efficient collaborative perception via information filling with codebook. In *Proceedings of the IEEE/CVF Conference on Computer Vision and Pattern Recognition*, pages 15481–15490, 2024. 1, 2
- [12] Tao Huang, Jianan Liu, Xi Zhou, Dinh C. Nguyen, Mostafa Rahimi Azghadi, Yuxuan Xia, Qing-Long Han, and Sumei Sun. Vehicle-to-everything cooperative perception for autonomous driving. *Proceedings of the IEEE*, 113(5):443–477, 2025. 1
- [13] Xun Huang, Jinlong Wang, Qiming Xia, Siheng Chen, Bisheng Yang, Xin Li, Cheng Wang, and Chenglu Wen. V2x-r: Cooperative lidar-4d radar fusion with denoising diffusion for 3d object detection. In *Proceedings of the Computer Vision and Pattern Recognition Conference*, pages 27390–27400, 2025. 5
- [14] Alex H Lang, Sourabh Vora, Holger Caesar, Lubing Zhou, Jiong Yang, and Oscar Beijbom. Pointpillars: Fast encoders for object detection from point clouds. In *Proceedings of the IEEE/CVF conference on computer vision and pattern recognition*, pages 12697–12705, 2019. 5
- [15] Zhiqi Li, Wenhai Wang, Hongyang Li, Enze Xie, Chonghao Sima, Tong Lu, Qiao Yu, and Jifeng Dai. Bevformer: learning bird’s-eye-view representation from lidar-camera via spatiotemporal transformers. *IEEE Transactions on Pattern Analysis and Machine Intelligence*, 2024. 1
- [16] Yen-Cheng Liu, Junjiao Tian, Nathaniel Glaser, and Zsolt Kira. When2com: Multi-agent perception via communication graph grouping. In *Proceedings of the IEEE/CVF Conference on computer vision and pattern recognition*, pages 4106–4115, 2020. 2
- [17] Yen-Cheng Liu, Junjiao Tian, Chih-Yao Ma, Nathan Glaser, Chia-Wen Kuo, and Zsolt Kira. Who2com: Collaborative perception via learnable handshake communication. In *2020 IEEE International Conference on Robotics and Automation (ICRA)*, pages 6876–6883. IEEE, 2020. 2
- [18] Yifan Lu, Quanhao Li, Baoan Liu, Mehrdad Dianati, Chen Feng, Siheng Chen, and Yanfeng Wang. Robust collaborative 3d object detection in presence of pose errors. In *2023 IEEE International Conference on Robotics and Automation (ICRA)*, pages 4812–4818. IEEE, 2023. 5
- [19] Jiageng Mao, Shaoshuai Shi, Xiaogang Wang, and Hongsheng Li. 3d object detection for autonomous driving: A comprehensive survey. *International Journal of Computer Vision*, 131(8):1909–1963, 2023. 1
- [20] Zican Shi, Jing Hu, Jie Ren, Hengkang Ye, Xuyang Yuan, Yan Ouyang, Jia He, Bo Ji, and Junyu Guo. Hs-fpn: High frequency and spatial perception fpn for tiny object detection. In *Proceedings of the AAAI Conference on Artificial Intelligence*, pages 6896–6904, 2025. 3
- [21] Sanbao Su, Songyang Han, Yiming Li, Zhili Zhang, Chen Feng, Caiwen Ding, and Fei Miao. Collaborative multi-object tracking with conformal uncertainty propagation. *IEEE Robotics and Automation Letters*, 9(4):3323–3330, 2024. 2
- [22] Tao Tang, Chaokun Zhang, Gong Chen, et al. Rocooper: Robust cooperative perception under vehicle-to-vehicle communication impairments. In *IEEE INFOCOM 2025-IEEE Conference on Computer Communications*, pages 1–10. IEEE, 2025. 2
- [23] Binglu Wang, Lei Zhang, Zhaozhong Wang, Yongqiang Zhao, and Tianfei Zhou. Core: Cooperative reconstruction

- for multi-agent perception. In *Proceedings of the IEEE/CVF International Conference on Computer Vision*, pages 8710–8720, 2023. 1, 2
- [24] Haohan Wang, Xindi Wu, Zeyi Huang, and Eric P Xing. High-frequency component helps explain the generalization of convolutional neural networks. In *Proceedings of the IEEE/CVF conference on computer vision and pattern recognition*, pages 8684–8694, 2020. 3
- [25] Tsun-Hsuan Wang, Sivabalan Manivasagam, Ming Liang, Bin Yang, Wenyuan Zeng, and Raquel Urtasun. V2vnet: Vehicle-to-vehicle communication for joint perception and prediction. In *European conference on computer vision*, pages 605–621. Springer, 2020. 2, 5
- [26] Shuang Wu, Guoqi Li, Lei Deng, Liu Liu, Dong Wu, Yuan Xie, and Luping Shi.  $l_1$ -norm batch normalization for efficient training of deep neural networks. *IEEE transactions on neural networks and learning systems*, 30(7):2043–2051, 2018. 2
- [27] Junhao Xu, Yanan Zhang, Zhi Cai, and Di Huang. Cosdh: Communication-efficient collaborative perception via supply-demand awareness and intermediate-late hybridization. In *Proceedings of the Computer Vision and Pattern Recognition Conference (CVPR)*, pages 6834–6843, 2025. 2, 5
- [28] Runsheng Xu, Hao Xiang, Zhengzhong Tu, Xin Xia, Ming-Hsuan Yang, and Jiaqi Ma. V2x-vit: Vehicle-to-everything cooperative perception with vision transformer. In *European conference on computer vision*, pages 107–124. Springer, 2022. 2, 5
- [29] Runsheng Xu, Hao Xiang, Xin Xia, Xu Han, Jinlong Li, and Jiaqi Ma. Opv2v: An open benchmark dataset and fusion pipeline for perception with vehicle-to-vehicle communication. In *2022 International Conference on Robotics and Automation (ICRA)*, pages 2583–2589. IEEE, 2022. 2, 5
- [30] Chenyu Yang, Yuntao Chen, Hao Tian, Chenxin Tao, Xizhou Zhu, Zhaoxiang Zhang, Gao Huang, Hongyang Li, Yu Qiao, Lewei Lu, et al. Bevfomer v2: Adapting modern image backbones to bird’s-eye-view recognition via perspective supervision. In *Proceedings of the IEEE/CVF conference on computer vision and pattern recognition*, pages 17830–17839, 2023. 1
- [31] Dingkan Yang, Kun Yang, Yuzheng Wang, Jing Liu, Zhi Xu, Rongbin Yin, Peng Zhai, and Lihua Zhang. How2comm: Communication-efficient and collaboration-pragmatic multi-agent perception. *Advances in Neural Information Processing Systems*, 36:25151–25164, 2023. 1, 2, 5
- [32] Haibao Yu, Yizhen Luo, Mao Shu, Yiyi Huo, Zebang Yang, Yifeng Shi, Zhenglong Guo, Hanyu Li, Xing Hu, Jirui Yuan, et al. Dair-v2x: A large-scale dataset for vehicle-infrastructure cooperative 3d object detection. In *Proceedings of the IEEE/CVF conference on computer vision and pattern recognition*, pages 21361–21370, 2022. 5
- [33] Jingyu Zhang, Kun Yang, Yilei Wang, Hanqi Wang, Peng Sun, and Liang Song. Ermvp: Communication-efficient and collaboration-robust multi-vehicle perception in challenging environments. In *Proceedings of the IEEE/CVF Conference on Computer Vision and Pattern Recognition*, pages 12575–12584, 2024. 1, 2, 5
- [34] Jingyu Zhang, Yilei Wang, Lang Qian, Peng Sun, Zengwen Li, Sudong Jiang, Maolin Liu, and Liang Song. Dsrc: Learning density-insensitive and semantic-aware collaborative representation against corruptions. In *Proceedings of the AAAI Conference on Artificial Intelligence*, pages 9942–9950, 2025. 1, 5